 CMES, vol.22, no.2, pp.129-149, 2007

Envelope frequency Response Function Analysis of Mechanical Structures with Uncertain Modal Damping Characteristics

D. Moens[1], **M. De Munck and D. Vandepitte**

Abstract: Recently, an interval finite element methodology has been developed to calculate envelope frequency response functions of uncertain structures with interval parameters. The methodology is based on a hybrid interval implementation of the modal superposition principle. This hybrid procedure consists of a preliminary optimization step, followed by an interval arithmetic procedure. The final envelope frequency response functions have been proved to give a very good approximation of the actual response range of the interval problem. Initially, this method was developed for undamped structures. Based on the theoretical principles of this approach, this paper introduces a new method for the analysis of structures with uncertain modal damping factors. In the proposed procedure, next to the classical interval parameters that affect stiffness and mass properties of the model, additional independent modal damping parameter intervals describe the uncertainty on the damping factor of each mode that is taken into account in the response function. The algorithm adopts the general modal superposition strategy of the undamped procedure. The effect of the introduction of the modal damping intervals in the interval arithmetic part of the procedure is studied analytically, and a new interval arithmetic procedure is developed according to the observations from this study. In order to validate the procedure, it is applied to a realistic industrial model with geometric as well as modal damping uncertainty.

Keyword: envelope frequency response functions, interval finite element analysis, uncertainty

[1] Postdoctoral research fellow of the Research Foundation - Flanders (FWO - Vlaanderen)

1 Introduction

Non-deterministic approaches are gaining momentum in the field of finite element analysis. The ability to include non-deterministic properties is of great value for a design engineer. It enables realistic reliability assessment that incorporates the uncertain aspects of the design. Furthermore, the design can be optimized for robust behavior under varying external influences. Recently, criticism arises on the general application of the probabilistic concept in this context. Especially when objective information on the uncertainties is limited, the subjective probabilistic analysis result proves to be of little value, and does not justify its high computational cost (see e.g. [Elishakoff (2000); Moens and Vandepitte (2005)]). Consequently, alternative non-probabilistic concepts are used for non-deterministic finite element analysis, as interval of fuzzy finite element analysis. Fuzzy finite element analysis forms the core of possibilistic analysis, which has been applied for non-probabilistic reliability studies [Stroud, Krishnamurthy, and Smith (2002)].

The Interval FE (IFE) analysis is based on the interval concept for the description of non-deterministic model properties, and so far has been studied only in limited publications (see e.g. [Köylüoğlu, Çakmak, and Nielsen (1995); Mullen and Muhanna (1999); Dessombz, Thouverez, Laîné, and Jézéquel (2001); Qiu, Wang, and Chen (2006)]). Recently, Muhanna introduced a penalty-based solution procedure for the IFE analysis [Muhanna, Mullen, and Zhang (2005)]. Also, new developments in the area of linear systems with interval parameters have been proposed by Neumaier [Neumaier (2006)]. The Fuzzy FE (FFE) analysis is basically an extension of the IFE analysis. It was first introduced by

Rao [Rao and Sawyer (1995)]. It has been studied in a number of specific research domains, as e.g. static structural analysis (see [Hanss (2003); Massa, Tison, and Lallemand (2006)]) and dynamic analysis (see [Chen and Rao (1997); Wasfy and Noor (1998); Donders, Vandepitte, Van de Peer, and Desmet (2005)]).

Recently, an interval finite element methodology to calculate envelope frequency response functions (FRF) of uncertain structures has been developed by the authors [Moens and Vandepitte (2004)]. This procedure forms the basis for the implementation of the fuzzy finite element method. The goal of the interval analysis is to calculate the envelope of the FRF taking into account that the input uncertainties can vary within the bounded space defined by their combined intervals. For this purpose, a hybrid procedure involving both a global optimization step and an interval arithmetic step has been developed. The resulting envelope response function gives a clear view on the possible variation of the response in the frequency domain.

While the efficiency and accuracy of the envelope FRF procedure has been proved, the method in its current form has an important shortcoming, as it cannot handle uncertainty on the damping properties of the analyzed model. Performing a realistic quantification of damping properties of a physical mechanical structure is generally not straightforward. This is mainly due to unknown internal characteristics of the used materials. But also the connecting parts in assemblies of components tend to have a high yet fairly unpredictable effect on the damping characteristics of a mechanical structure. Generally, the lack of information on damping properties forms a major source of non-determinism, especially in the dynamic response analysis of structures. Therefore, the possible extension of the proposed envelope FRF procedure toward the analysis of structures with imprecise damping properties constitutes a fundamental extension of the applicability and practical value of the dynamic interval finite element analysis.

Section 2 of this work first summarizes the undamped envelope FRF procedure as it was initially developed in [Moens and Vandepitte (2004)]. The effect of the introduction of independent modal parameter intervals on the procedure is then analyzed in section 3. Finally, section 4 illustrates the newly developed procedure by applying it on a realistic case study.

2 Envelope FRF analysis of undamped structures

The goal of the envelope FRF analysis is to calculate the bounds on the dynamic response of a structure in a specific frequency region given that a set of model parameters $\mathbf{x}$ is uncertain but bounded. The intervals on these parameters are specified in an interval vector $\mathbf{x}^{\mathbf{I}}$. The methodology for the envelope dynamic response analysis as developed by the authors is based on a hybrid interval solution strategy, consisting of a preliminary optimization step, followed by an interval arithmetic step. In the first part of this procedure, the optimization is used to translate the interval properties defined on the finite element model to the exact interval modal stiffness and mass parameters of the structure. The calculation of the envelope FRFs in the second part is done by applying the interval arithmetic equivalent of the modal superposition procedure on these interval modal parameters. The final envelope FRFs have been proved to contain only a very limited amount of conservatism. A brief overview of the basic principles of the method is given in this section. The complete mathematical description of the method can be found in [Moens and Vandepitte (2004)].

2.1 The deterministic modal superposition principle

For undamped structures, the deterministic modal superposition principle states that, considering the first n_{modes} modes, the frequency response function between degrees of freedom j and k equals:

$$FRF_{jk} = \sum_{i=1}^{n_{modes}} FRF_{jk}^{i} = \sum_{i=1}^{n_{modes}} \frac{\phi_{i_j}\phi_{i_k}}{\phi_{\mathbf{i}}{}^{T}\mathbf{K}\phi_{\mathbf{i}} - \omega^2\phi_{\mathbf{i}}{}^{T}\mathbf{M}\phi_{\mathbf{i}}} \tag{1}$$

with $\phi_{\mathbf{i}}$ the i^{th} eigenvector of the system and ϕ_{i_j} the j^{th} component of the i^{th} eigenvector. Simplifi-

cation of Eq. 1 yields:

$$FRF_{jk} = \sum_{i=1}^{n_{modes}} \frac{1}{\hat{k}_i - \omega^2 \hat{m}_i} \tag{2}$$

with $\hat{k}_i$ and $\hat{m}_i$ the modal parameters defined as:

$$\hat{k}_i = \frac{\boldsymbol{\phi_i}^T \mathbf{K} \boldsymbol{\phi_i}}{\phi_{i_j} \phi_{i_k}} = \frac{1}{\phi_{i_j}^K \phi_{i_k}^K} \tag{3}$$

$$\hat{m}_i = \frac{\boldsymbol{\phi_i}^T \mathbf{M} \boldsymbol{\phi_i}}{\phi_{i_j} \phi_{i_k}} = \frac{1}{\phi_{i_j}^M \phi_{i_k}^M} \tag{4}$$

with $\boldsymbol{\phi}_\mathbf{i}^\mathbf{K}$ and $\boldsymbol{\phi}_\mathbf{i}^\mathbf{M}$ the stiffness and mass normalized eigenvectors of the system.

2.2 Interval finite element FRF analysis

The modal superposition principle has been translated into an interval finite element method for FRF analysis. Figure 1 gives a graphical overview of the translation of the deterministic algorithm into an interval procedure. On the left-hand side is the deterministic algorithm as described in the previous section. On the right-hand side is the same procedure translated to an equivalent interval algorithm.

The interval method consists of the calculation of the result ranges of the sub functions appearing in the consecutive steps of the deterministic algorithm. Therefore, the deterministic algorithm is split into three sub functions. In the first step, step 1.1, the modal stiffness $\hat{k}_i$ and mass $\hat{m}_i$ are calculated for each considered mode. Step 1.2 then consists of the calculation of the modal FRF contributions FRF_{jk}^i. Step 1.1 and 1.2 have to be performed for each mode that is taken into consideration in the modal superposition. Therefore, it is referred to as the *modal part*. In step 2, the superposition is performed by a summation of the modal FRF contributions.

The interval procedure follows the same outline as the deterministic algorithm. Each step now concentrates on the derivation of the range of the sub functions in the deterministic algorithm:

step 1.1 For all n_{modes} taken into account, the ranges of possible values that the modal stiffness and mass can adopt have to be determined, taking into account that the uncertain parameters in $\mathbf{x}$ can vary within their respective intervals. These correct ranges of the modal parameters denoted by $\hat{k}_i^S$ and $\hat{m}_i^S$ are determined using a minimization and maximization over the uncertain interval space $\mathbf{x}^\mathbf{I}$. For numerical convenience, the global optimization is performed on the inverted modal parameters, after which the obtained intervals are inverted in order to obtain the actual modal parameter ranges:

$$\hat{k}_i^S = \left[\min_{\mathbf{x} \in \mathbf{x}^\mathbf{I}} \left(\phi_{i_j}^K \phi_{i_k}^K \right), \max_{\mathbf{x} \in \mathbf{x}^\mathbf{I}} \left(\phi_{i_j}^K \phi_{i_k}^K \right) \right]^{-1} \tag{5}$$

$$\hat{m}_i^S = \left[\min_{\mathbf{x} \in \mathbf{x}^\mathbf{I}} \left(\phi_{i_j}^M \phi_{i_k}^M \right), \max_{\mathbf{x} \in \mathbf{x}^\mathbf{I}} \left(\phi_{i_j}^M \phi_{i_k}^M \right) \right]^{-1} \tag{6}$$

If the inverted modal parameter range contains zero, the inversion results in the union of two interval ranging from respectively plus and minus infinity to a finite value. These modes are referred to as *switch modes*. The modes for which the inverted modal parameter interval has a constant sign, are referred to as *strict modes*, and classified in either positive or negative modes, based on the sign of the interval.

step 1.2 The modal envelope FRF is calculated by substituting the ranges of the modal parameters in the deterministic expression of the modal FRF contribution:

$$\left(FRF_{jk}^i\right)^I = \frac{1}{\hat{k}_i^S - \omega^2 \hat{m}_i^S} \tag{7}$$

This is an analytical procedure performed using the interval arithmetic approach.

step 2 Finally, the total interval FRF is obtained by the summation of the contributions of all considered modes:

$$FRF_{jk}^I = \sum_{i=1}^{n} \left(FRF_{jk}^i\right)^I \tag{8}$$

Also this final step is performed using interval arithmetics.

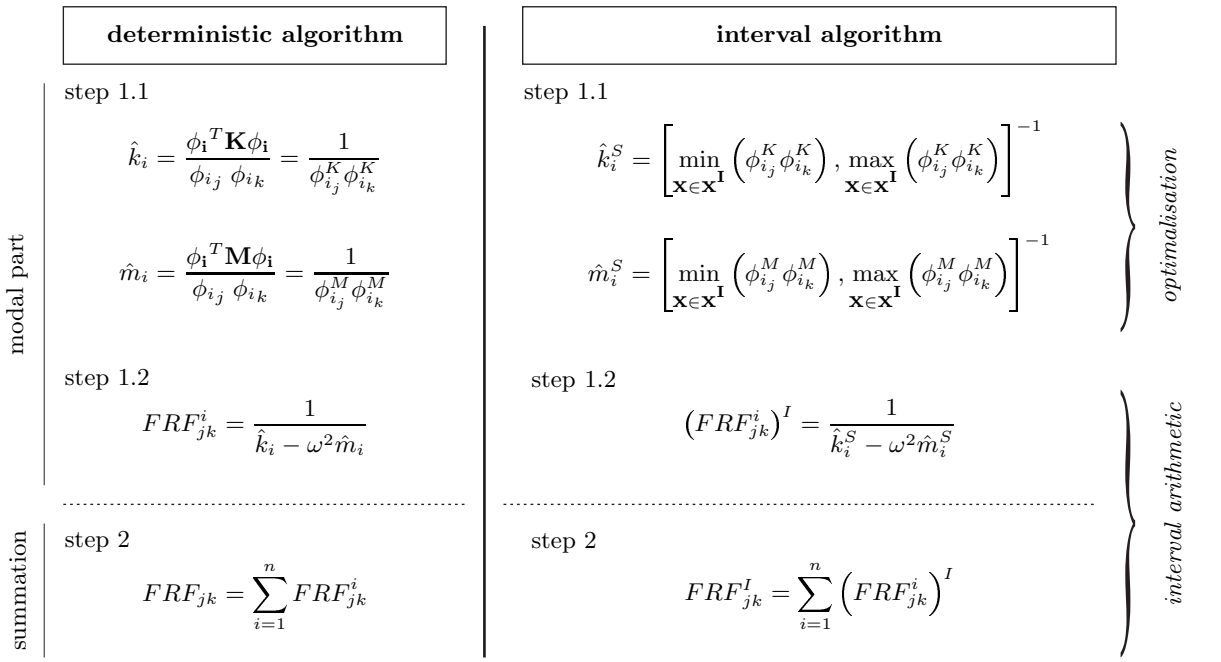

Figure 1: Translation of the deterministic modal superposition algorithm to an equivalent interval procedure

2.3 Eigenvalue interval correction

The method as described above is enhanced based on a graphical interpretation of the modal part of the interval algorithm. For each mode, consider the domain of modal mass and stiffness pairs that are achieved by considering the complete range of models defined by the interval uncertainty space $\mathbf{x}^{\mathbf{I}}$:

$$\langle \hat{k}_i, \hat{m}_i \rangle = \left\{ \left(\hat{k}_i, \hat{m}_i \right) \mid \left(\mathbf{x} \in \mathbf{x}^{\mathbf{I}} \right) \right\} \tag{9}$$

This domain defines a bounded area in a $\hat{k}_i, \hat{m}_i$-workspace. The exact bounds of this domain however, are generally unknown. The modal part of the interval algorithm now is interpreted in this workspace. From the optimization as described in step 1.1, it is clear that, for a strict mode, the calculated ranges on the modal parameters $\hat{k}_i^S$ and $\hat{m}_i^S$ represent a rectangular approximation of the actual $\langle \hat{k}_i, \hat{m}_i \rangle$-domain. Therefore, this method is referred to as the *Modal Rectangle* (MR) method. Figure 2 shows a general $\langle \hat{k}_i, \hat{m}_i \rangle$-domain and its approximation using the MR method.

The interval arithmetic procedure for the calculation of the modal envelope FRF contributions in step 1.2 is interpreted in the same graphical domain. The goal in this step is to derive the bounds on the deterministic modal FRF, taking into account that $\hat{k}_i$ and $\hat{m}_i$ are located anywhere inside their intervals. By considering the modal FRF contribution as defined in Eq. 7 as an analytical function of $\hat{k}_i$ and $\hat{m}_i$, the bounds on this function over the modal rectangle have to be determined. It has been shown that this can be done analytically for the complete frequency domain, by considering only the function evaluations at the upper left and the lower right corner points of the rectangle. For switch modes, the modal domain spans

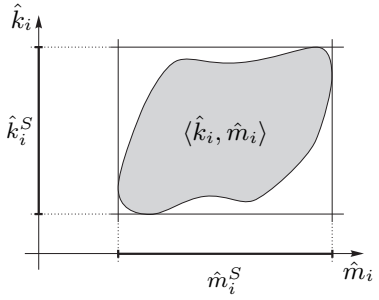

Figure 2: Graphical illustration of a mode's $\langle \hat{k}_i, \hat{m}_i \rangle$-domain and its approximation using the modal rectangle method

out over the first and third quadrant of the modal parameter space. Still, a similar interpretation is possible (see [Moens and Vandepitte (2004)]).

Based on these observations, it becomes clear that the calculation based on the modal rectangle introduces conservatism in the procedure if the actual $\langle \hat{k}_i, \hat{m}_i \rangle$-domain differs strongly from the approximate rectangle. This is often the case, as the modal parameters are generally strongly coupled through the global system and therefore show a high degree of correlation. Therefore, an enhanced procedure has been introduced. The enhancement is based on an improved approximation of the $\langle \hat{k}_i, \hat{m}_i \rangle$-domain. This is achieved by using information on the eigenvalue ranges, which are obtained using an additional eigenvalue optimization step in the modal part of the algorithm. An eigenvalue interval λ_i^I introduces an extra restriction on the quotient of possible combinations of the modal parameters. This restriction is mathematically expressed as:

$$\underline{\lambda_i} \leq \frac{\hat{k}_i}{\hat{m}_i} \leq \overline{\lambda_i} \tag{10}$$

Graphically, the eigenvalue bounds represent lines through the origin of the $\hat{k}_i, \hat{m}_i$-space tangent to the actual $\langle \hat{k}_i, \hat{m}_i \rangle$-domain. These lines are extra delimiters for the $\langle \hat{k}_i, \hat{m}_i \rangle$-domain approximation, and therefore give rise to an improved $\langle \hat{k}_i, \hat{m}_i \rangle$-domain approximation as illustrated in figure 3. This domain is referred to as the *Modal Rectangle with Eigenvalue interval correction* (MRE).

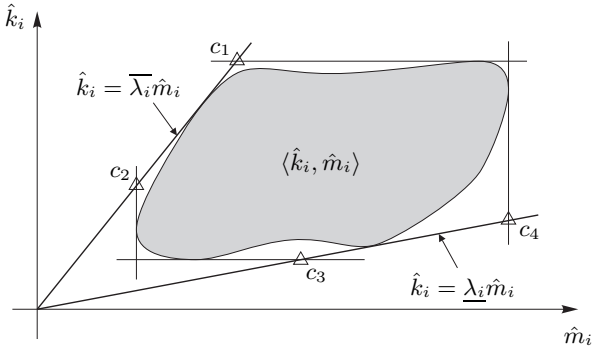

Figure 3: Effect of the introduction of the exact eigenvalue interval in the $\langle \hat{k}_i, \hat{m}_i \rangle$-domain approximation of a positive mode

It has been shown that the conservatism in the modal envelope FRF contributions derived in step 1.2 is substantially reduced by considering the MRE domain instead of the MR domain as area of possible modal parameter pairs. The corresponding modal envelope FRF contributions are determined analytically by calculating the deterministic modal FRFs at the vertex points of the MRE-domain (indicated with c_i, $i = 1 \ldots 4$ in figure 3). This yields:

$$\left(FRF_{jk}^{i}\right)^{I} = \begin{cases} \left[\dfrac{\overline{\lambda_i}}{\overline{\hat{k}_i}\left(\overline{\lambda_i} - \omega^2\right)}, \dfrac{\underline{\lambda_i}}{\underline{\hat{k}_i}\left(\underline{\lambda_i} - \omega^2\right)}\right] & \text{for } \omega^2 \leq \underline{\lambda_i} \\ \left[\dfrac{\overline{\lambda_i}}{\overline{\hat{k}_i}\left(\overline{\lambda_i} - \omega^2\right)}, \dfrac{1}{\overline{\hat{m}_i}\left(\underline{\lambda_i} - \omega^2\right)}\right] & \text{for } \underline{\lambda_i} < \omega^2 < \overline{\lambda_i} \\ \left[\dfrac{1}{\underline{\hat{m}_i}\left(\overline{\lambda_i} - \omega^2\right)}, \dfrac{1}{\overline{\hat{m}_i}\left(\underline{\lambda_i} - \omega^2\right)}\right] & \text{for } \overline{\lambda_i} \leq \omega^2 \end{cases} \tag{11}$$

for positive modes, and:

$$\left(FRF_{jk}^{i}\right)^{I} = \begin{cases} \left[\dfrac{\underline{\lambda_i}}{\overline{\hat{k}_i}\left(\underline{\lambda_i} - \omega^2\right)}, \dfrac{\overline{\lambda_i}}{\underline{\hat{k}_i}\left(\overline{\lambda_i} - \omega^2\right)}\right] & \text{for } \omega^2 \leq \underline{\lambda_i} \\ \left[\dfrac{1}{\underline{\hat{m}_i}\left(\underline{\lambda_i} - \omega^2\right)}, \dfrac{\overline{\lambda_i}}{\underline{\hat{k}_i}\left(\overline{\lambda_i} - \omega^2\right)}\right] & \text{for } \underline{\lambda_i} < \omega^2 < \overline{\lambda_i} \\ \left[\dfrac{1}{\underline{\hat{m}_i}\left(\underline{\lambda_i} - \omega^2\right)}, \dfrac{1}{\overline{\hat{m}_i}\left(\overline{\lambda_i} - \omega^2\right)}\right] & \text{for } \overline{\lambda_i} \leq \omega^2 \end{cases} \tag{12}$$

for negative modes. A similar procedure was derived for the bounds on the modal FRF contributions of switch modes. It has been shown that after applying the final summation step, this enhancement on the modal level of the algorithm leads to a close and guaranteed outer approximation of the actual modal envelope FRF contribution [Moens and Vandepitte (2004)].

3 Introduction of independent modal damping intervals in the envelope FRF procedure

3.1 Overview of the algorithm

For damped structures with modal damping parameters $\hat{c}_i$ defined for each mode taken into consideration, the modal superposition procedure states that the total FRF equals:

$$FRF_{jk} = \sum_{i=1}^{n} \frac{1}{\hat{k}_i + j\hat{c}_i\omega - \omega^2\hat{m}_i} \tag{13}$$

$$= \sum_{i=1}^{n} FRF_{jk}^{i} \tag{14}$$

with FRF_{jk}^{i} the i^{th} modal FRF and $\hat{k}_i$ and $\hat{m}_i$ the normalized modal parameters as defined in equations Eq. 3 and Eq. 4, and $\hat{c}_i$ the corresponding modal damping parameter, expressed as:

$$\hat{c}_i = 2\eta_i\sqrt{\hat{k}_i\hat{m}_i} \tag{15}$$

using η_i in its classical definition as the modal damping ratio.

Equation 13 shows that the damped FRF calculation through the modal superposition principle is very similar to the undamped case. Compared to the undamped FRF, the main difference caused by the addition of damping is that the modal FRF contributions FRF_{jk}^{i} are complex functions. Also, the modal damping parameter $\hat{c}_i$ appears explicitly in the expression of the modal contributions. Again, the strategy for the calculation of the range of the modal contributions is based on the definition of a domain of possible modal parameters. The evolution of the real and imaginary part of a modal contribution over this domain then determines the envelope bounds of both parts.

For the modal mass and stiffness parameters, the feasible domain is inherited from the undamped MRE-concept as described in section 2.3. The MRE $\langle\hat{k}_i,\hat{m}_i\rangle$-domain has to be extended in order to take the damping uncertainty into account. By placing an interval on the modal damping ratio for each mode, an interval on the modal damping parameters is obtained using Eq. 15. This means that the two-dimensional MRE $\langle\hat{k}_i,\hat{m}_i\rangle$-domain is extended in a third dimension in which the modal damping parameter range is represented. As this modal damping interval is implemented as an independent model uncertainty, it has no relation with the other modal parameters. Hence, the extension in this third dimension comes down to an extrusion of the existing MRE $\langle\hat{k}_i,\hat{m}_i\rangle$-domain over the interval defined for the corresponding modal damping parameter. Figure 4 illustrates the resulting polyhedron in the new three dimensional modal $\left(\hat{k}_i,\hat{m}_i,\hat{c}_i\right)$-space.

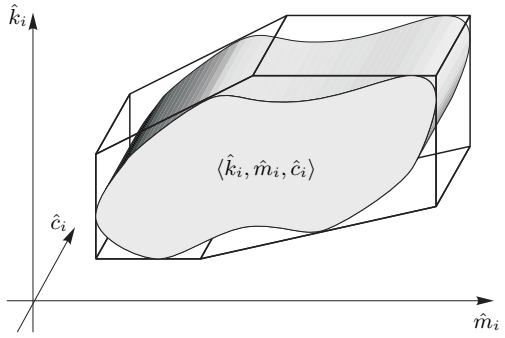

Figure 4: Graphical representation of the approximation of the $\langle\hat{k}_i,\hat{m}_i,\hat{c}_i\rangle$-domain after addition of the independent modal damping interval to the MRE $\langle\hat{k}_i,\hat{m}_i\rangle$-domain approximation

Now that we have an outer approximation of the modal $\langle\hat{k}_i,\hat{m}_i,\hat{c}_i\rangle$-domain, the range of the modal contributions FRF_{jk} as defined in Eq. 13 have to be calculated. The algorithm processes the real and complex parts of the response separately. For both parts, the response range is calculated for each mode. The superposition then constructs the range of the real and imaginary parts of the total response by adding together all real respectively imaginary modal FRF contributions. Finally, based on these results, the amplitude and phase are directly derived from the total real and imaginary envelope FRFs.

In summary, the outline of the MRE algorithm extended to structures with modal damping uncertainties is the following:

1. for all considered modes:
   (a) calculate the MRE $\langle\hat{k}_i,\hat{m}_i\rangle$-domain approximation by calculating the range of

the modal mass and stiffness parameters and the eigenfrequency

(b) derive the intervals on the modal damping parameters based on modal damping ratio intervals

(c) calculate the range of the modal real and imaginary FRF based on the MRE $\langle \hat{k}_i, \hat{m}_i, \hat{c}_i \rangle$-domain approximation

2. sum the modal real and imaginary envelope FRFs to obtain a conservative approximation of the total real and imaginary envelope FRFs

3. post-process the real and imaginary parts to obtain the total amplitude and phase envelope FRF

Step 1a is completely similar to the undamped case (see section 2.3 or [Moens and Vandepitte (2004)] for details). Also, step 1b is straightforward, and results directly from the definition of the treated problem. The core of the theoretical development is in step 1c which consists of the analytical derivation of the modal real and imaginary envelope FRFs given the MRE $\langle \hat{k}_i, \hat{m}_i, \hat{c}_i \rangle$-domain approximation as illustrated in figure 4. Sections 3.1.1 and 3.1.2 describe these in detail for a positive mode. Sections 3.1.3 and 3.1.4 describe how to obtain the equivalent procedure for negative respectively switch modes. The final processing of the real and imaginary parts to the amplitude and phase envelopes is briefly summarized in section 3.2.

3.1.1 Modal real envelope FRF calculation for positive modes

The real part of the modal FRF in Eq. 13 equals:

$$\Re\left(FRF^i_{jk}\right) = \frac{\hat{k}_i - \omega^2 \hat{m}_i}{\left(\hat{k}_i - \omega^2 \hat{m}_i\right)^2 + \hat{c}_i^2 \omega^2} \tag{16}$$

This is further referred to as the modal real FRF. At a specific frequency ω, it can be regarded as an analytical function of the three modal parameters $\hat{k}_i$, $\hat{m}_i$ and $\hat{c}_i$. The range of this function taking into account that the modal parameters are inside the used polyhedral $\langle \hat{k}_i, \hat{m}_i, \hat{c}_i \rangle$-domain approximation is now derived analytically.

A first important observation is made regarding the evolution of the modal real FRF for $\left(\hat{k}_i, \hat{m}_i, \hat{c}_i\right)$-locations on a line parallel to the $\hat{c}_i$-axis in the modal parameter space. By taking the derivative of the real part function in the $\hat{c}_i$-direction at constant values for $\hat{m}_i$ and $\hat{k}_i$, it is easily shown that the real part function always evolves monotonically over these lines. Therefore, in order to find the bounds on the range of this function over these lines, only the lower and upper bound of the modal damping parameter interval have to be taken into consideration. This means that the global bounds of the real part response function over the polyhedral $\langle \hat{k}_i, \hat{m}_i, \hat{c}_i \rangle$-domain can be calculated by analyzing the $\left(\hat{k}_i, \hat{m}_i, \hat{c}_i\right)$-locations in the two-dimensional MRE domains at $\hat{c}_i = \underline{\hat{c}_i}$ and $\hat{c}_i = \overline{\hat{c}_i}$.

The behavior of the real part response function over horizontal, vertical and sloped lines in the two-dimensional MRE domain at a specific modal damping value c^* is now first analyzed. This will lead to the the procedure for the calculation of the modal real envelope FRF described at the end of this section.

Lines parallel to the $\hat{k}_i$-axis For the analysis of the behavior of the modal real FRF for modal parameter combinations on vertical lines (parallel to the $\hat{k}_i$-axis) in the modal parameter space, the constant values m^* and c^* are introduced for the modal mass and damping parameters in Eq. 16. This results in a function $\Re\left(FRF^i_{jk}\right)_{m^*,c^*}$ which has only $\hat{k}_i$ as variable. The analysis now focuses on the variation of this function when the modal stiffness parameter varies over a positive interval $\left[\underline{k}, \overline{k}\right]$. It can be shown that the modal real FRF as a function of $\hat{k}_i$ has exactly one minimum and one maximum as illustrated in figure 5. The extrema are reached for $\hat{k}_i$ equal to respectively:

$$k_+(\omega) = m^* \omega^2 + c^* \omega \tag{17}$$

$$k_-(\omega) = m^* \omega^2 - c^* \omega \tag{18}$$

The explicit function of ω indicates that the locations of the extrema depend on the frequency.

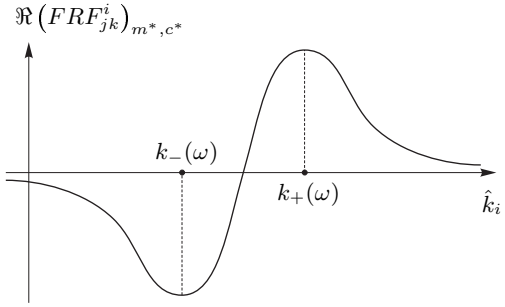

Figure 5: Evolution of the modal real FRF over the $\hat{k}_i$ domain for a constant modal mass and damping value

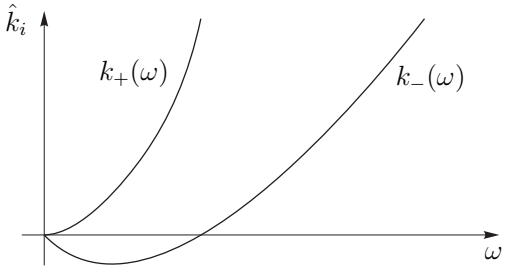

Figure 6: Evolution of $k_-(\omega)$ and $k_+(\omega)$ in the frequency domain

Figure 6 illustrates the global form of both the location of the maximum $k_+(\omega)$ and the minimum $k_-(\omega)$ as a function of the frequency.

Both functions start in the origin of the $\hat{k}_i$-axis. This means that for low frequencies, both extrema in figure 5 are located to the left-hand side of any positive $\left[\underline{k},\overline{k}\right]$ interval on the $\hat{k}_i$-axis. For increasing frequency, both extrema approach and possibly cross the interval. This can be interpreted as if the response function of figure 5 evolves globally to the right relative to the $\left[\underline{k},\overline{k}\right]$ interval. The implications of this evolution for the lower and upper bound of the response is discussed by analyzing the frequency domain in increasing direction.

- The lower response bound:
  For small frequencies, both extrema are situated to the left of the $\left[\underline{k},\overline{k}\right]$ interval. Therefore, the lower bound on the real response corresponds to the upper bound of the interval as indicated in figure 7(a). When the frequency increases, the response function shifts to the right and the response maximum enters the $\left[\underline{k},\overline{k}\right]$ interval. Further, a frequency is reached for which the response values are equal for $\underline{k}$ and $\overline{k}$ (figure 7(b)). From this frequency on, the response minimum is located on the lower bound of the $\left[\underline{k},\overline{k}\right]$ interval (figure 7(c)). When the frequency increases further, the response minimum enters the $\left[\underline{k},\overline{k}\right]$ interval for some frequency. Starting from this frequency, the response minimum is located in the extremum inside the $\left[\underline{k},\overline{k}\right]$ interval (figure 7(d)) and the minimal value of the response is obtained for the corresponding $k_-(\omega)$ values. Finally, the response minimum reaches the upper bound of the interval for some frequency. From this frequency on, the function over the interval becomes monotonically decreasing and the response minimum is located in the upper bound of the interval (figure 7(e)).

- The upper response bound:
  For small frequencies, both extrema are situated to the left of the $\left[\underline{k},\overline{k}\right]$ interval. Therefore, the upper bound on the response corresponds to the lower bound of the interval as indicated in figure 7(a). Since $k_+(\omega)$ is monotonically increasing, the location of the response maximum always enters the $\left[\underline{k},\overline{k}\right]$ interval for some frequency. Starting from this frequency, the response maximum is located in the extremum inside the $\left[\underline{k},\overline{k}\right]$ interval (figure 7(b)). For these frequencies, the maximal value of the response is obtained for the corresponding $k_+(\omega)$ values. Once the response maximum has reached the upper bound of the $\left[\underline{k},\overline{k}\right]$ interval, the response maximum is located in the upper bound of the interval (figure 7(c)). When the frequency increases further, the response minimum enters the $\left[\underline{k},\overline{k}\right]$ interval. A frequency is reached for which the response values are equal for $\underline{k}$ and $\overline{k}$ (figure 7(d)). From this frequency on, the response maximum is located on the lower bound of the $\left[\underline{k},\overline{k}\right]$ interval (figure 7(e)).

This description shows that the exact upper and lower bounds on the modal real FRF above an

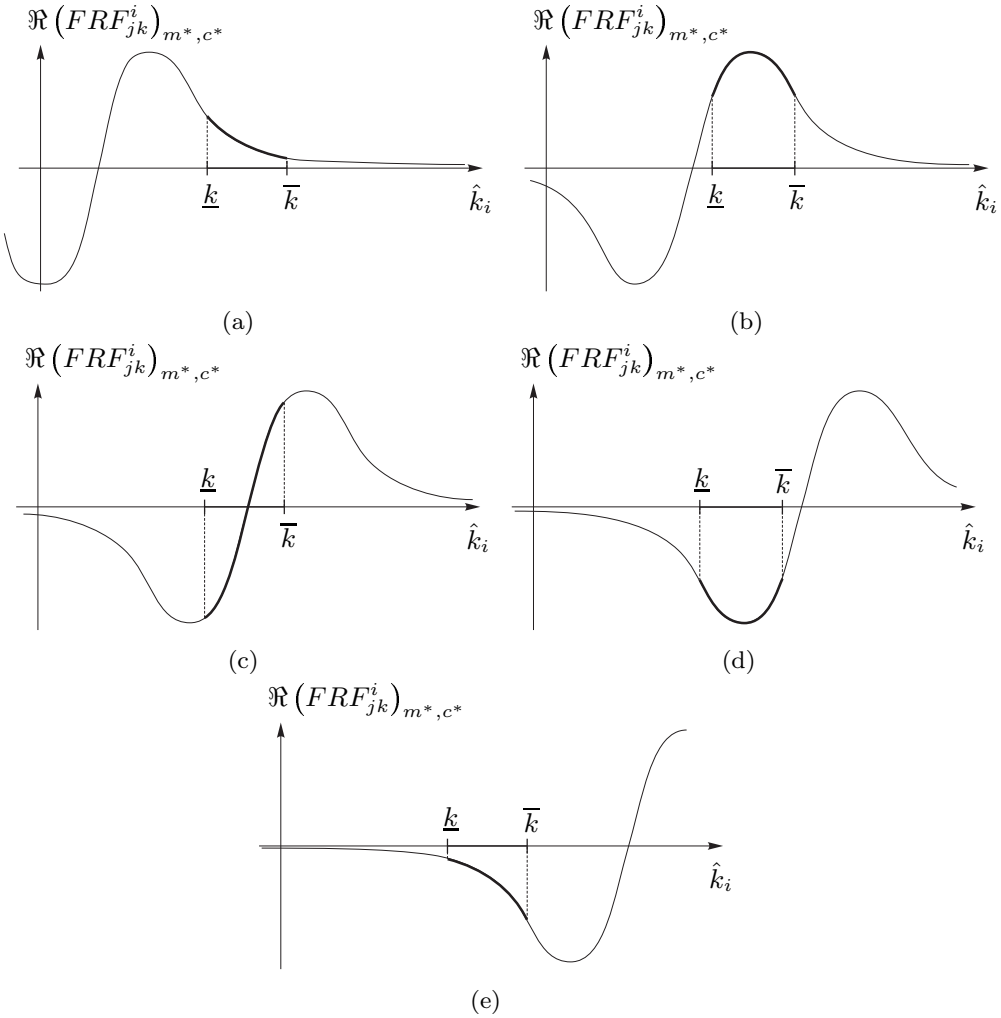

Figure 7: (a)-(e) Evolution of the modal real FRF above an interval on a vertical line in the modal parameter space for increasing frequencies

interval on a vertical line in the modal parameter space follow directly from an analytical procedure. The procedure consists of selecting the correct $\hat{k}_i$ value which, combined with the m^* value at the vertical line, yields the bounds of the modal real FRF at c^*. This correct $\hat{k}_i$ value always lies either on one of the bounds of the $\left[\underline{k},\overline{k}\right]$ interval, either in an extremum of the modal real FRF inside the interval. The evolution of this $\hat{k}_i$ value as a function of ω is illustrated in figure 8(a) for the lower bound and in figure 8(b) for the upper bound.

The frequencies ω_1^l, ω_2^l, ω_1^u and ω_2^u represent the points where respectively $k_-(\omega)$ and $k_+(\omega)$ cross with $\hat{k}_i = \underline{k}$ and $\hat{k}_i = \overline{k}$. Therefore, they satisfy:

$$\underline{k} = m^* {\omega_1^l}^2 - c^* \omega_1^l \tag{19}$$

$$\overline{k} = m^* {\omega_2^l}^2 - c^* \omega_2^l \tag{20}$$

$$\underline{k} = m^* {\omega_1^u}^2 + c^* \omega_1^u \tag{21}$$

$$\overline{k} = m^* {\omega_2^u}^2 + c^* \omega_2^u \tag{22}$$

Furthermore, $\omega_=^l$ and $\omega_=^u$ follow directly from satisfying the equation:

$$\Re\left(FRF^i_{jk}(\omega_=)\right)_{\underline{k},m^*,c^*} = \Re\left(FRF^i_{jk}(\omega_=)\right)_{\overline{k},m^*,c^*} \tag{23}$$

This means that the curves of $\hat{k}_i$ values that yield the bounds on the response at any frequency ω as

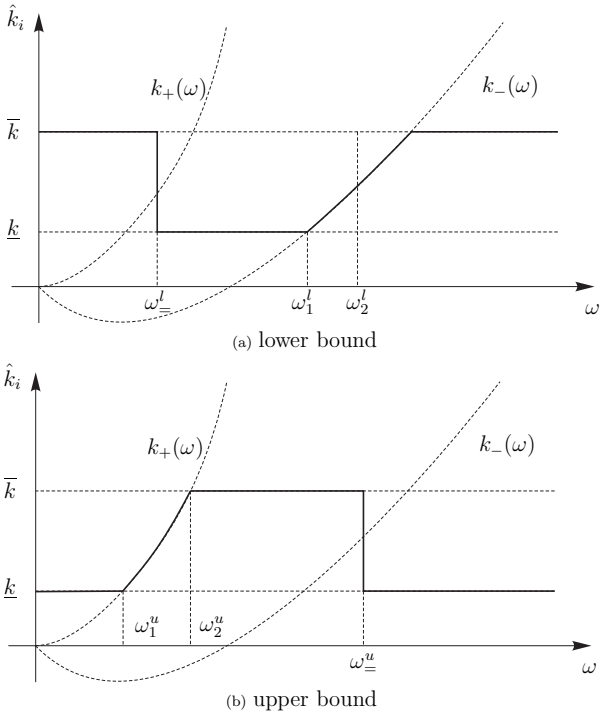

Figure 8: Evolution of the $\hat{k}_i$ value corresponding to the extrema of the modal real FRF at a vertical line in the modal parameter space - (a) lower bound (b) upper bound

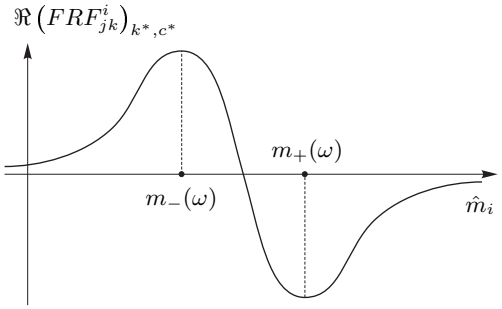

Figure 9: Evolution of the modal real FRF over the $\hat{m}_i$ domain for a constant modal mass and damping value

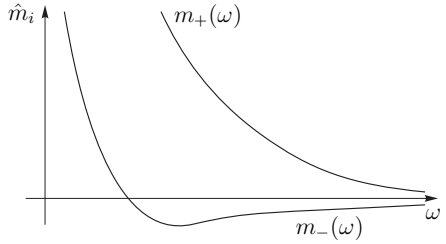

Figure 10: Evolution of $m_-(\omega)$ and $m_+(\omega)$ in the frequency domain

given in figure 8 are completely described analytically. Hence, the bounds on the real FRF over the vertical line can be calculated by substituting the values on this curves into Eq. 16.

Lines parallel to the $\hat{m}_i$-axis The procedure to calculate the bounds on the modal real FRF above a horizontal line in the modal parameter space is very similar to the one for the vertical lines described above. Constant values k^* and c^* are introduced for the modal stiffness and damping parameters in Eq. 16. This results in a function $\Re\left(FRF_{jk}^i\right)_{k^*,c^*}$ which has only $\hat{m}_i$ as variable. When the modal mass parameter varies over a positive interval $[\underline{m},\overline{m}]$, the modal real FRF as a function of $\hat{m}_i$ has exactly one minimum and one maximum as illustrated in figure 9. The extrema are reached for $\hat{m}_i$ equal to respectively:

$$m_+(\omega) = \frac{k^*}{\omega^2} + \frac{c^*}{\omega} \tag{24}$$

$$m_-(\omega) = \frac{k^*}{\omega^2} - \frac{c^*}{\omega} \tag{25}$$

Also here, the locations of the extrema depend on the frequency as illustrated in figure 10. Both functions tend to infinity at $\omega = 0$, and tend to zero when ω tends to infinity.

The implications of the evolution of $m_-(\omega)$ and $m_+(\omega)$ for the lower and upper bound of the response is similar to the description for the vertical boundary in figure 7. The difference is that in this case the locations of the extrema decrease for increasing ω and that the minimum and maximum have switched positions. Still, the exact upper and lower bounds on the modal real FRF above an interval on a horizontal line in the modal parameter space follow directly from a similar analytical procedure. The procedure consists of selecting the correct $\hat{m}_i$ value which, combined with the k^* and c^* value at the horizontal line, yields the lower and upper bound of the modal real FRF. The evolution of this correct $\hat{m}_i$ value as a function of ω is illustrated in figure 11(a) for the lower bound and in figure 11(b) for the upper bound.

Again, the curves in figure 11 are fully described analytically, as the frequencies ω_1^l, ω_2^l, ω_1^u and

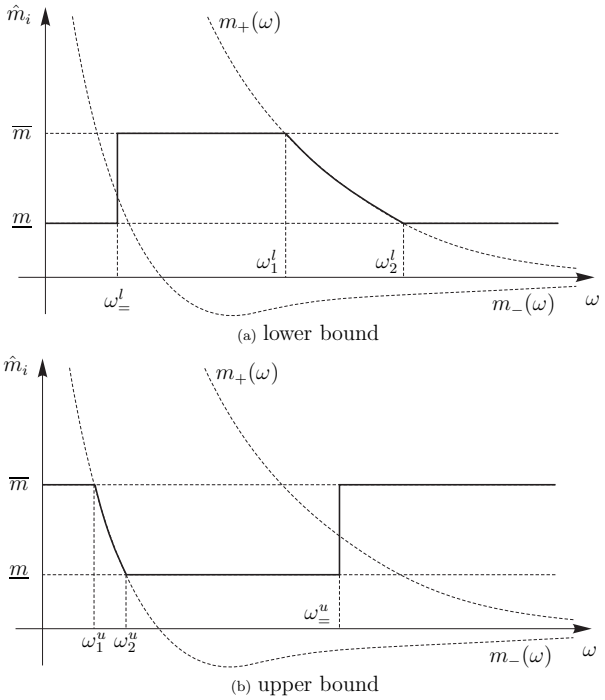

(a) lower bound

(b) upper bound

Figure 11: Evolution of the $\hat{m}_i$ value corresponding to the extrema of the modal real FRF at a horizontal line in the modal parameter space - (a) lower bound. (b) upper bound

ω_2^u represent the points where respectively $m_+(\omega)$ and $m_-(\omega)$ cross with $\hat{m}_i = \overline{m}$ and $\hat{m}_i = \underline{m}$, and $\omega_=^l$ and $\omega_=^u$ follow directly from satisfying:

$$\Re\left(FRF_{jk}^i(\omega_=)\right)_{\underline{m},k^*,c^*} = \Re\left(FRF_{jk}^i(\omega_=)\right)_{\overline{m},k^*,c^*} \tag{26}$$

Lines with a constant slope in the modal parameter space The bounds on the modal real FRF above a line with a constant slope are derived analytically. In Eq. 16, a constant value c^* is introduced for the modal damping parameter. The sloped line is represented by introducing $\hat{k}_i = \lambda^* \hat{m}_i$ into the same equation. This results in the function:

$$\Re\left(FRF_{jk}^i\right) = \frac{\hat{m}_i(\lambda^* - \omega^2)}{\hat{m}_i^2(\lambda^* - \omega^2)^2 + \hat{c}_i^2\omega^2} \tag{27}$$

which has only $\hat{m}_i$ as variable. The analysis now focuses on the variation of this function when the modal mass parameter varies over a positive interval $[\underline{m}, \overline{m}]$. Similar as for the horizontal and vertical lines in the modal parameter space, it can be shown that the modal real FRF as a function of $\hat{m}_i$ has exactly one minimum and one maximum. The extrema are reached for $\hat{m}_i$ equal to respectively:

$$m_+^\lambda(\omega) = \frac{c^*\omega}{\lambda^* - \omega^2} \tag{28}$$

$$m_-^\lambda(\omega) = \frac{c^*\omega}{\omega^2 - \lambda^*} \tag{29}$$

Also here, the explicit function of ω indicates that the locations of the extrema vary with the frequency. In this case however, the exact evolution of these extrema strongly depends on the gradient of the slope λ^*. Similar to the horizontal and vertical lines, the extrema of the modal real FRF will be reached either on the bounds of the interval $[\underline{m}, \overline{m}]$, or on the extrema for the frequencies for which the functions $m_+(\omega)$ and $m_-(\omega)$ are located within the interval $[\underline{m}, \overline{m}]$. Therefore, the following procedure is applied:

1. (a) calculate the modal real FRF given in Eq. 27 for all frequencies at the lower and upper bounds of $\hat{m}_i$, resulting respectively in $\Re\left(FRF_{jk}^i\right)_{\underline{m}}$ and $\Re\left(FRF_{jk}^i\right)_{\overline{m}}$
   (b) calculate the modal real FRF given in Eq. 27 at $m_+^\lambda(\omega_+)$ and $m_-^\lambda(\omega_-)$ with:
   $$\omega_+ = \{\omega \mid \underline{m} < m_+^\lambda(\omega) < \overline{m}\} \tag{30}$$
   $$\omega_- = \{\omega \mid \underline{m} < m_-^\lambda(\omega) < \overline{m}\} \tag{31}$$
   resulting respectively in $\Re\left(FRF_{jk}^i\right)_{m_+^\lambda}$ and $\Re\left(FRF_{jk}^i\right)_{m_-^\lambda}$
2. calculate the lower bound on the modal real FRF using:
   $$\min\left(\Re\left(FRF_{jk}^i\right)_{\underline{m}}, \Re\left(FRF_{jk}^i\right)_{\overline{m}}\right) \tag{32}$$
   for $\omega \notin \omega_-$, and
   $$\min\left(\Re\left(FRF_{jk}^i\right)_{\underline{m}}, \Re\left(FRF_{jk}^i\right)_{\overline{m}}, \Re\left(FRF_{jk}^i\right)_{m_-^\lambda}\right) \tag{33}$$
   for $\omega \in \omega_-$

3. calculate the upper bound on the modal real FRF using:

$$\max\left(\Re\left(FRF^i_{jk}\right)_{\underline{m}}, \Re\left(FRF^i_{jk}\right)_{\overline{m}}\right) \tag{34}$$

for $\omega \notin \omega_+$, and

$$\max\left(\Re\left(FRF^i_{jk}\right)_{\underline{m}}, \Re\left(FRF^i_{jk}\right)_{\overline{m}}, \Re\left(FRF^i_{jk}\right)_{m^\lambda_+}\right) \tag{35}$$

for $\omega \in \omega_+$

From these equations, the bounds on the modal real FRF are now determined for the complete frequency domain.

Minimum and maximum response locations in MRE $\langle \hat{k}_i, \hat{m}_i \rangle$-domain The analytical analysis of the modal real FRF over vertical and horizontal lines in the MRE $\langle \hat{k}_i, \hat{m}_i \rangle$-subdomain of the $\langle \hat{k}_i, \hat{m}_i, \hat{c}_i \rangle$-domain indicates that local optima are possibly present inside the domain. Figure 12 shows the locations k_+ and k_- of local optima of the modal real FRF on a vertical line at $\hat{m}_i = m^*$. The response value at the local optima locations on the line, however, proves to be independent of the location of the line. Indeed, as the local maximum of the modal real FRF at the frequency ω on a vertical line at (m^*, c^*) is found at $k_+(\omega)$, substituting $k_+(\omega)$ as defined in Eq. 17 together with m^* and c^* in Eq. 16 yields the response value at the local maximum:

$$\Re\left(FRF^i_{jk}\right)_{m^*,c^*,k_+} = \frac{1}{2c^*\omega} \tag{36}$$

Since this value is independent from m^*, the response value at the local maximum found on a vertical line in the domain does not depend on the location of the line. Consequently, the same maximum response value is reached at $(\hat{k}_i, \hat{m}_i)$-combinations located on the line represented by $k_+(\omega)$:

$$\hat{k}_i = \hat{m}_i\omega^2 + c^*\omega \tag{37}$$

This equation represents a straight line in the $\langle \hat{k}_i, \hat{m}_i \rangle$-domain, as indicated in figure 12. As this line crosses with the MRE $\langle \hat{k}_i, \hat{m}_i \rangle$-bounds, it is concluded that if a local maximum is reached inside the domain, it will also be present on the boundary lines of the domain. This observation can be generalized toward local minima. The line of constant local modal real FRF minimum is illustrated in figure 12, and yields:

$$\hat{k}_i = \hat{m}_i\omega^2 - c^*\omega \tag{38}$$

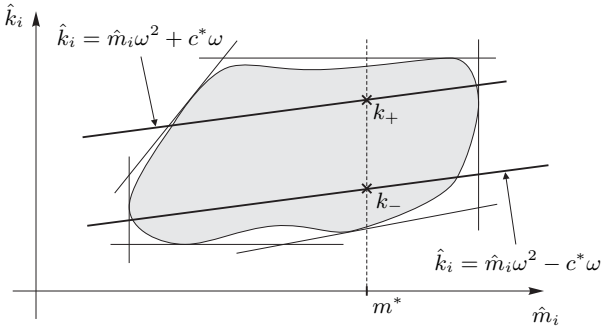

Figure 12: Locations of the local maximum of the modal real FRF at a vertical line at $\hat{m}_i = m^*$ and the corresponding lines of constant optima

In conclusion, we can state the if local optima are present inside the two-dimensional MRE subdomain, they are also present on the boundary lines of this subdomain. Therefore, the final procedure to derive the modal real FRF bounds focuses exclusively on the behavior of the modal real FRF above the MRE $\langle \hat{k}_i, \hat{m}_i \rangle$-domain boundary lines.

Modal real envelope FRF procedure In order to find the range of values that the modal real FRF can reach inside the polyhedral $\langle \hat{k}_i, \hat{m}_i, \hat{c}_i \rangle$-domain illustrated in figure 4, the following procedure applies:

1. for both the MRE $\langle \hat{k}_i, \hat{m}_i \rangle$-subdomains at $\underline{\hat{c}_i}$ and $\overline{\hat{c}_i}$:
   (a) analyze the optima of the modal real FRF for the vertical boundary lines
   (b) analyze the optima of the modal real FRF for the horizontal boundary lines

(c) analyze the optima of the modal real FRF for the sloped boundary lines representing the eigenvalue interval bounds

2. envelope the ranges of the modal real FRF obtained in the previous step

The implementation is done based on the definition of the MRE $\langle \hat{k}_i, \hat{m}_i \rangle$-domain as illustrated in figure 3. Step 1a is implemented by applying the vertical line procedure on the line segments at $\hat{m}_i = \underline{\hat{m}_i}$ and $\hat{m}_i = \overline{\hat{m}_i}$ with $\hat{k}_i$ ranging respectively from $\underline{\hat{k}_i}$ to $\underline{\hat{m}_i}\overline{\lambda_i}$ and from $\overline{\hat{m}_i}\underline{\lambda_i}$ to $\overline{\hat{k}_i}$. Step 1b is implemented by applying the horizontal line procedure on the line segments at $\hat{k}_i = \underline{\hat{k}_i}$ and $\hat{k}_i = \overline{\hat{k}_i}$ with $\hat{m}_i$ ranging respectively from $\underline{\hat{m}_i}$ to $\underline{\hat{k}_i}/\underline{\lambda_i}$ and from $\overline{\hat{k}_i}/\overline{\lambda_i}$ to $\overline{\hat{m}_i}$. Step 1c is implemented by applying the sloped line procedure with λ^* respectively equal to $\underline{\lambda_i}$ and $\overline{\lambda_i}$, and $\hat{m}_i$ ranging respectively from $\underline{\hat{k}_i}/\underline{\lambda_i}$ to $\overline{\hat{m}_i}$, and from $\underline{\hat{m}_i}$ to $\overline{\hat{k}_i}/\overline{\lambda_i}$.

Finally in step 2, the modal real FRF range for the complete $\langle \hat{k}_i, \hat{m}_i, \hat{c}_i \rangle$-domain is derived by taking the union of the modal real FRF envelopes found in the MRE $\langle \hat{k}_i, \hat{m}_i \rangle$-subdomains at both $\underline{\hat{c}_i}$ and $\overline{\hat{c}_i}$.

3.1.2 *Modal imaginary envelope FRF calculation for positive modes*

The imaginary part of the modal FRF in Eq. 13 equals:

$$\Im\left(FRF^i_{jk}\right) = \frac{-\hat{c}_i\omega}{\left(\hat{k}_i - \omega^2\hat{m}_i\right)^2 + \hat{c}_i^2\omega^2} \tag{39}$$

This is further referred to as the modal imaginary FRF. Also here, the range of this function taking into account that the modal parameters are inside the used polyhedral $\langle \hat{k}_i, \hat{m}_i, \hat{c}_i \rangle$-domain approximation is derived analytically by considering the behavior of the function over specific lines in the modal parameter space.

In this case, the domain of possible locations of extreme values of the modal imaginary FRF is reduced significantly by first considering radial lines in the $\left(\hat{k}_i, \hat{m}_i\right)$-space at a specific $\hat{c}_i$. It can be shown that on these lines, the modal imaginary FRF has a monotonic behavior with respect to the radial distance to the origin of the $\left(\hat{k}_i, \hat{m}_i\right)$-space. Referring to the global polyhedral form of the $\langle \hat{k}_i, \hat{m}_i, \hat{c}_i \rangle$-domain approximation as illustrated in figure 4, this means that no local optima are present inside the domain, neither on the planes resulting from extruding the MRE eigenvalue delimiters in the modal damping parameter direction. The analytical search for optima therefore is limited to the horizontal and vertical boundary planes of the $\langle \hat{k}_i, \hat{m}_i, \hat{c}_i \rangle$-domain. These planes are now analyzed by considering the lines on these planes parallel to the modal parameter axes.

Lines parallel to the $\hat{c}_i$-axis For the analysis of the behavior of the modal imaginary FRF for $\left(\hat{k}_i, \hat{m}_i, \hat{c}_i\right)$-locations on a line parallel to the $\hat{c}_i$-axis, constant values m^* and k^* are introduced for the modal mass and stiffness parameters in Eq. 39. This results in a function $\Im\left(FRF^i_{jk}\right)_{k^*,m^*}$ which has only $\hat{c}_i$ as variable. The analysis focuses on the variation of this function when $\hat{c}_i$ varies over a positive interval $[\underline{c}, \overline{c}]$. It can be shown that the modal imaginary FRF as a function of $\hat{c}_i$ has exactly one maximum and one minimum as illustrated in figure 13. The maximum and minimum are reached for $\hat{c}_i$ equal to respectively:

$$c_+(\omega) = \left|\frac{k^*}{\omega} - m^*\omega\right| \tag{40}$$

$$c_-(\omega) = -\left|\frac{k^*}{\omega} - m^*\omega\right| \tag{41}$$

It is clear that $c_-(\omega)$ is negative for all frequencies. Therefore, it is not of importance in the derivation of the response bounds over a positive $[\underline{c}, \overline{c}]$ interval. Figure 14 illustrates the global form of the evolution of $c_+(\omega)$ over the frequency domain.

The exact upper and lower bounds on the modal imaginary FRF above an interval on the analyzed line in the modal parameter space follow directly from an analytical procedure. The $\hat{c}_i$-values for which the upper and lower bounds on the response are reached are always located either on one of the bounds of the $[\underline{c}, \overline{c}]$ interval, or in the extremum locations c_+ or c_- inside the interval. The evolution

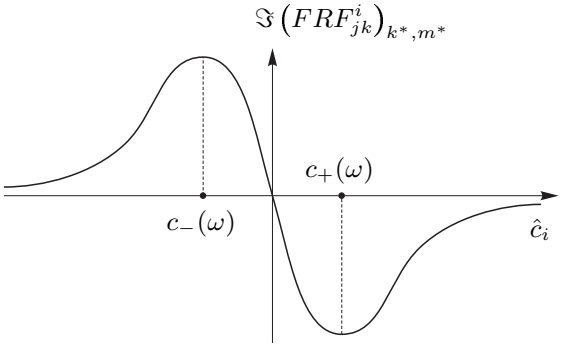

Figure 13: Evolution of the modal imaginary FRF over the $\hat{c}_i$ domain for a constant modal stiffness and mass value

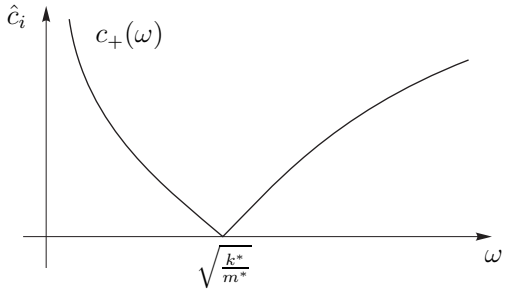

Figure 14: Evolution of $c_+(\omega)$ in the frequency domain

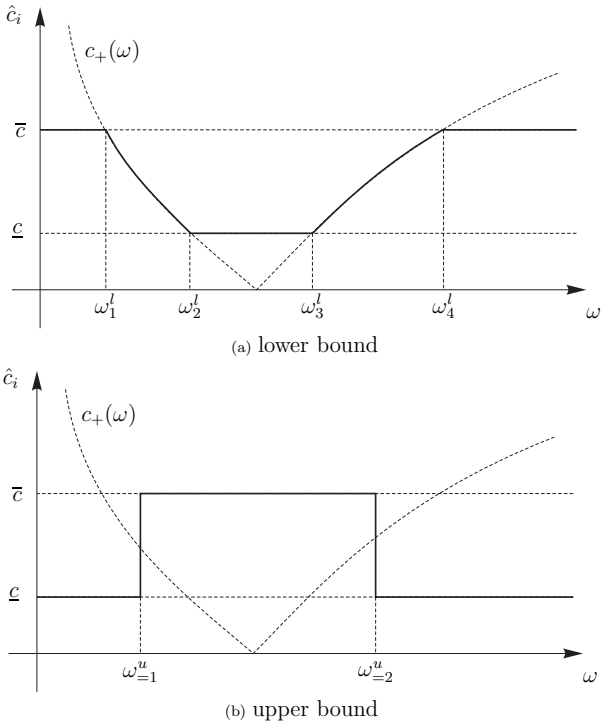

Figure 15: Evolution of the $\hat{c}_i$ value corresponding to the extrema of the modal imaginary FRF at the analyzed line in the modal parameter space - (a) lower bound (b) upper bound.

of this optimal $\hat{c}_i$ value as a function of ω is illustrated in figure 15(a) for the lower bound and in figure 15(b) for the upper bound.

The frequencies ω^l_1 and ω^l_2 represent the lower points where $c_+(\omega)$ crosses respectively with $\hat{m}_i = \overline{m}$ and $\hat{m}_i = \underline{m}$. Similarly, the frequencies ω^l_3 and ω^l_4 represent the upper points where $c_+(\omega)$ crosses respectively with $\hat{m}_i = \overline{m}$ and $\hat{m}_i = \underline{m}$. Therefore, they satisfy:

$$\overline{c} = \frac{k^*}{\omega^l_1} - m^*\omega^l_1 \tag{42}$$

$$\underline{c} = \frac{k^*}{\omega^l_2} - m^*\omega^l_2 \tag{43}$$

$$\underline{c} = m^*\omega^l_3 - \frac{k^*}{\omega^l_3} \tag{44}$$

$$\overline{c} = m^*\omega^l_4 - \frac{k^*}{\omega^l_4} \tag{45}$$

Furthermore, $\omega^u_{=1}$ and $\omega^u_{=2}$ follow directly as the two roots resulting from the equation:

$$\Im\left(FRF^i_{jk}(\omega^u_=)\right)_{\underline{c},k^*,m^*} = \Im\left(FRF^i_{jk}(\omega^u_=)\right)_{\overline{c},k^*,m^*} \tag{46}$$

This means that the curves of optimal $\hat{c}_i$ values given in figure 15 are completely described analytically, and the bounds on the imaginary FRF over the analyzed line can be calculated by substituting the values on these curves into Eq. 39.

Lines parallel to the $\hat{k}_i$-axis The introduction of constant values m^* and c^* for the modal mass and damping parameters in equation (39) results in a function $\Im\left(FRF^i_{jk}\right)_{m^*,c^*}$ which has only $\hat{k}_i$ as variable. If $\hat{k}_i$ varies over a positive interval $\left[\underline{k},\overline{k}\right]$, the modal imaginary FRF as a function of $\hat{k}_i$ has exactly one minimum as illustrated in figure 16. This minimum is reached for $\hat{k}_i$ equal to:

$$k_1(\omega) = m^*\omega^2 \tag{47}$$

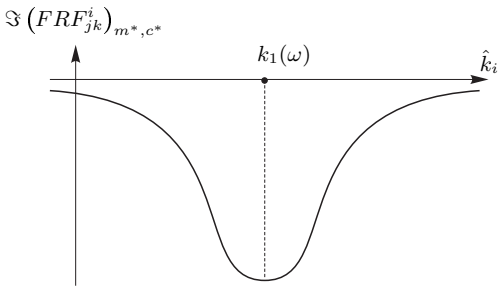

Figure 16: Evolution of the modal imaginary FRF over the $\hat{k}_i$ domain for a constant modal mass and damping value

The location of the minimum $k_1(\omega)$ is a monotonically increasing function of the frequency.

Again, the exact upper and lower bounds on the modal imaginary FRF above an interval on the analyzed $\hat{k}_i$-line in the modal parameter space follow directly from an analytical procedure. The evolution of the $\hat{k}_i$ values that yield the bounding functions of the response range is illustrated in figure 17(a) for the lower bound and in figure 17(b) for the upper bound.

The frequencies ω_1^l and ω_2^l represent the points where $k_1(\omega)$ crosses respectively with $\hat{k}_i = \underline{k}$ and $\hat{k}_i = \overline{k}$. Therefore, they equal:

$$\omega_1^l = \sqrt{\frac{\underline{k}}{m^*}} \tag{48}$$

$$\omega_2^l = \sqrt{\frac{\overline{k}}{m^*}} \tag{49}$$

Furthermore, $\omega_=^u$ follows directly from satisfying the equation:

$$\Im\left(FRF^i_{jk}(\omega_=^u)\right)_{\underline{k},m^*,c^*} = \Im\left(FRF^i_{jk}(\omega_=^u)\right)_{\overline{k},m^*,c^*} \tag{50}$$

which yields:

$$\omega_=^u = \sqrt{\frac{\underline{k}+\overline{k}}{2m^*}} \tag{51}$$

This means that the curves of optimal $\hat{k}_i$ values given in figure 17 are completely described analytically, and the bounds on the imaginary FRF

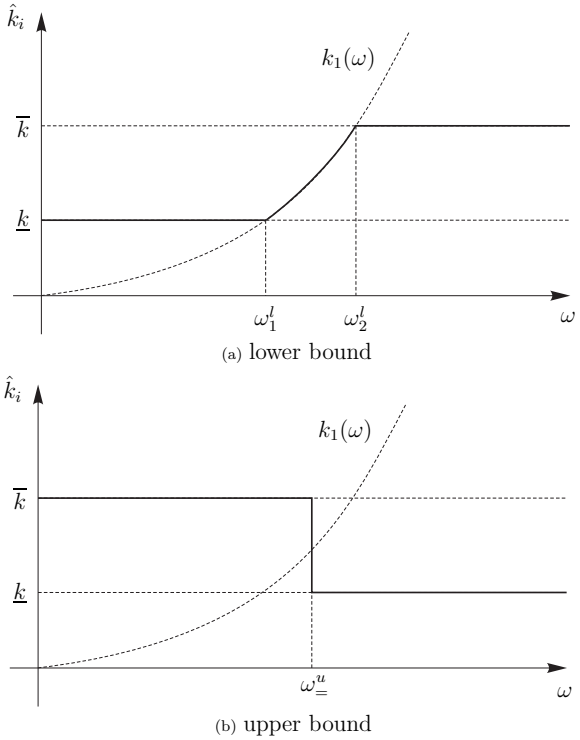

Figure 17: Evolution of the $\hat{k}_i$ value corresponding to the extrema of the modal imaginary FRF at the analyzed line in the modal parameter space - (a) lower bound. (b) upper bound

over the analyzed line can be calculated by substituting the values on these curves into equation (39).

Lines parallel to the $\hat{m}_i$-axis For the analysis of the behavior of the modal imaginary FRF for $\left(\hat{k}_i, \hat{m}_i, \hat{c}_i\right)$-locations on lines parallel to the $\hat{m}_i$-axis, constant values k^* and c^* are introduced for the modal stiffness and damping parameters in equation (39). This results in a function $\Im\left(FRF^i_{jk}\right)_{k^*,c^*}$ which has only $\hat{m}_i$ as variable. Again, it can be shown that when $\hat{m}_i$ varies over a positive interval $[\underline{m}, \overline{m}]$, the modal imaginary FRF as a function of $\hat{m}_i$ has exactly one minimum as illustrated in figure 18. This minimum is reached for $\hat{m}_i$ equal to:

$$m_1(\omega) = \frac{k^*}{\omega^2} \tag{52}$$

The location of the minimum $m_1(\omega)$ starts from infinity at $\omega = 0$ after which it tends to zero when

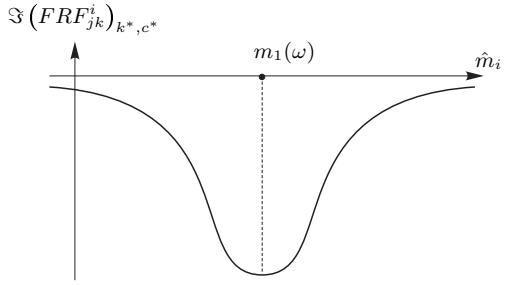

Figure 18: Evolution of the modal imaginary FRF over the $\hat{m}_i$ domain for a constant modal stiffness and damping value

the frequency tends to infinity.

The exact upper and lower bounds on the modal imaginary FRF above the analyzed line in the modal parameter space follow directly from an analytical procedure. The evolution of the $\hat{m}_i$ values that yield the bounding functions of the response range is illustrated in figure 19(a) for the lower bound and in figure 19(b) for the upper bound.

The frequencies ω_1^l and ω_2^l represent the points where $m_1(\omega)$ crosses respectively with $\hat{m}_i = \overline{m}$ and $\hat{m}_i = \underline{m}$. Therefore, they equal:

$$\omega_1^l = \sqrt{\frac{k^*}{\overline{m}}} \tag{53}$$

$$\omega_2^l = \sqrt{\frac{k^*}{\underline{m}}} \tag{54}$$

Furthermore, $\omega_=^u$ follows directly from satisfying the equation:

$$\Im\left(FRF^i_{jk}(\omega_=^u)\right)_{\underline{m},k^*,c^*} = \Im\left(FRF^i_{jk}(\omega_=^u)\right)_{\overline{m},k^*,c^*} \tag{55}$$

which yields:

$$\omega_=^u = \sqrt{\frac{2k^*}{\underline{m}+\overline{m}}} \tag{56}$$

This means that the curves of optimal $\hat{m}_i$ values given in figure 19 are completely described analytically, and the bounds on the imaginary FRF over the analyzed line can be calculated by substituting the values on this curves into equation (39).

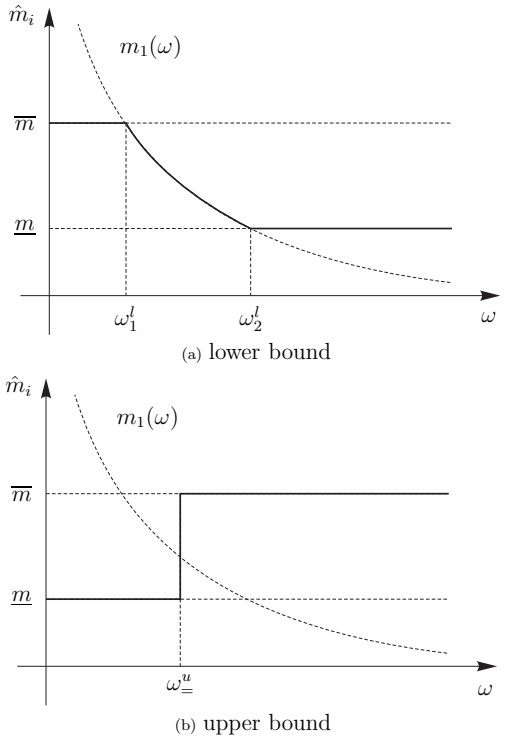

(a) lower bound

(b) upper bound

Figure 19: Evolution of the $\hat{m}_i$ value corresponding to the extrema of the modal imaginary FRF at the analyzed line in the modal parameter space - (a) lower bound (b) upper bound.

Minimum and maximum response locations on horizontal and vertical planes The analytical analysis of the modal imaginary FRF over lines parallel to the $\hat{c}_i$-axis in the $\langle \hat{k}_i, \hat{m}_i, \hat{c}_i \rangle$-domain indicates that a local minimum is possibly present inside the considered $\left[\underline{\hat{c}_i}, \overline{\hat{c}_i}\right]$ interval. The response value at the local minimum, however, proves to be independent of the location of the line. Indeed, if the location of the local minimum is not on the boundary of the domain, it is found at $c_+(\omega)$. Substituting $c_+(\omega)$ as defined in Eq. 40, m^* and k^* in Eq. 39 yields:

$$\Im\left(FRF^i_{jk}\right)_{m^*,k^*,c_+} = -\frac{1}{2c^*\omega} \tag{57}$$

Since this value is independent from both m^* and k^*, the response value at the local minimum found on a line parallel to the $\hat{c}_i$-axis does not depend on the location of the line. Hence, in order to find the range of the modal imaginary FRF over a horizontal or vertical plane in the $\left(\hat{k}_i, \hat{m}_i, \hat{c}_i\right)$-space,

only the boundary lines of these planes have to be analyzed.

Modal imaginary envelope FRF procedure The procedure for the analytical response range analysis of the modal imaginary FRF is the following:

1. analyze the optima of the modal imaginary FRF for the $\langle \hat{k}_i, \hat{m}_i, \hat{c}_i \rangle$-domain boundary lines parallel to the $\hat{c}_i$-axis
2. analyze the optima of the modal imaginary FRF for the vertical boundary lines of the polyhedral $\langle \hat{k}_i, \hat{m}_i, \hat{c}_i \rangle$-domain approximation
3. analyze the optima of the modal imaginary FRF for the horizontal boundary lines of the polyhedral $\langle \hat{k}_i, \hat{m}_i, \hat{c}_i \rangle$-domain approximation
4. envelope the ranges of the modal imaginary FRF obtained in the previous steps

The implementation is done based on the definition of the MRE $\langle \hat{k}_i, \hat{m}_i \rangle$-domain as illustrated in figure 3 and its extrusion in the $\hat{c}_i$-direction as illustrated in figure 4. Step 1 is implemented based on the analysis on lines parallel to the $\hat{c}_i$-axis described above at the lines with the following (k^*, m^*)-locations: $(\underline{\hat{k}_i}, \underline{\hat{m}_i})$, $(\underline{\hat{m}_i}\overline{\lambda_i}, \underline{\hat{m}_i})$, $(\overline{\hat{k}_i}, \overline{\hat{k}_i}/\overline{\lambda_i})$, $(\overline{\hat{k}_i}, \overline{\hat{m}_i})$, $(\overline{\hat{m}_i}\underline{\lambda_i}, \overline{\hat{m}_i})$ and $(\underline{\hat{k}_i}, \underline{\hat{k}_i}/\underline{\lambda_i})$. Step 2 is implemented by applying the vertical line procedure on the line segments at $\hat{m}_i = \underline{\hat{m}_i}$ and $\hat{m}_i = \overline{\hat{m}_i}$ with $\hat{k}_i$ ranging respectively from $\underline{\hat{k}_i}$ to $\underline{\hat{m}_i}\overline{\lambda_i}$ and from $\overline{\hat{m}_i}\underline{\lambda_i}$ to $\overline{\hat{k}_i}$, both at $\underline{\hat{c}_i}$ and $\overline{\hat{c}_i}$. Step 3 is implemented by applying the horizontal line procedure on the line segments at $\hat{k}_i = \underline{\hat{k}_i}$ and $\hat{k}_i = \overline{\hat{k}_i}$ with $\hat{m}_i$ ranging respectively from $\underline{\hat{m}_i}$ to $\underline{\hat{k}_i}/\underline{\lambda_i}$ and from $\overline{\hat{k}_i}/\overline{\lambda_i}$ to $\overline{\hat{m}_i}$, both at $\underline{\hat{c}_i}$ and $\overline{\hat{c}_i}$. Finally in step 4, the modal imaginary FRF range for the complete $\langle \hat{k}_i, \hat{m}_i, \hat{c}_i \rangle$-domain is derived by taking the union of the modal imaginary FRF envelopes found in the previous steps.

3.1.3 The modal envelope FRF for negative modes

The analytical procedures in sections 3.1.1 and 3.1.2 consider only positive ranges for the modal parameters. They require that the $\langle \hat{k}_i, \hat{m}_i, \hat{c}_i \rangle$-domain approximations of the analyzed modes are located in the first quadrant of the modal parameter space, and, therefore, are limited to positive modes. The goal is to apply these procedures also for negative modes. This can be achieved by considering the MRE $\langle \hat{k}_i, \hat{m}_i, \hat{c}_i \rangle$-domain approximation of a negative mode mirrored into the first quadrant of the modal parameter space. This is equivalent with switching the sign of the modal parameters. The corresponding horizontal and vertical boundaries on the mirrored modal parameters are then:

$$\overline{-\hat{k}_i} = -(\underline{\hat{k}_i}) \tag{58}$$

$$\underline{-\hat{k}_i} = -(\overline{\hat{k}_i}) \tag{59}$$

$$\overline{-\hat{m}_i} = -(\underline{\hat{m}_i}) \tag{60}$$

$$\underline{-\hat{m}_i} = -(\overline{\hat{m}_i}) \tag{61}$$

$$\overline{-\hat{c}_i} = -(\underline{\hat{c}_i}) \tag{62}$$

$$\underline{-\hat{c}_i} = -(\overline{\hat{c}_i}) \tag{63}$$

It is easily shown that for negative modes, the correct modal real and imaginary envelope FRFs are obtained by compensating for the modal parameter sign inversion in the following way:

$$\underline{\Re\left(FRF^i_{jk}\right)_{\hat{k}_i,\hat{m}_i,\hat{c}_i}} = -\left(\overline{\Re\left(FRF^i_{jk}\right)_{-\hat{k}_i,-\hat{m}_i,-\hat{c}_i}}\right) \tag{64}$$

$$\overline{\Re\left(FRF^i_{jk}\right)_{\hat{k}_i,\hat{m}_i,\hat{c}_i}} = -\left(\underline{\Re\left(FRF^i_{jk}\right)_{-\hat{k}_i,-\hat{m}_i,-\hat{c}_i}}\right) \tag{65}$$

for the real part, and:

$$\underline{\Im\left(FRF^i_{jk}\right)_{\hat{k}_i,\hat{m}_i,\hat{c}_i}} = -\left(\overline{\Im\left(FRF^i_{jk}\right)_{-\hat{k}_i,-\hat{m}_i,-\hat{c}_i}}\right) \tag{66}$$

$$\overline{\Im\left(FRF^i_{jk}\right)_{\hat{k}_i,\hat{m}_i,\hat{c}_i}} = -\left(\underline{\Im\left(FRF^i_{jk}\right)_{-\hat{k}_i,-\hat{m}_i,-\hat{c}_i}}\right) \tag{67}$$

for the imaginary part. The conclusion is that with an appropriate pre- and post-processing of

the data used in and obtained from the procedures for the positive modes, the equivalent procedure for the negative modes is easily implemented.

3.1.4 The modal envelope FRF for switch modes

For a switch mode, the MRE $\langle \hat{k}_i, \hat{m}_i \rangle$-domain approximation ranges over infinity in the modal parameter space. It is easily shown that both the modal real and imaginary FRF tend to zero when the modal parameters tend to infinity inside the MRE $\langle \hat{k}_i, \hat{m}_i \rangle$-domain approximation. Therefore, the ranges of the modal real and imaginary FRF should contain zero for all frequencies. Therefore, the procedure consists of the following steps:

1. the calculation of the upper and lower bounds on the modal real and imaginary FRF for the MRE $\langle \hat{k}_i, \hat{m}_i, \hat{c}_i \rangle$-domain approximation both in the first and the third quadrant

2. taking the maximum of all upper bounds and minimum of all lower bounds of the envelope functions resulting from the previous step

3. the calculation of the modal real and imaginary envelope FRFs by correcting positive lower bounds and negative upper bounds in the result of the previous step to zero

The derivation of the range of the modal FRFs in step 1 results from applying the procedure for positive and negative modes described above to the finite boundaries in respectively the first and third quadrant of the MRE $\langle \hat{k}_i, \hat{m}_i, \hat{c}_i \rangle$-domain approximation of the switch mode.

3.2 Total amplitude and phase envelope FRF calculation

After the calculation of the modal real and imaginary envelope FRF of all modes, the total amplitude and phase envelope FRF are calculated using the total real and imaginary envelope FRFs. These result from the summation of the modal contributions derived in the previous sections:

$$\Re\left(FRF_{jk}\right)^I = \sum_{i=1}^{n} \Re\left(FRF_{jk}^i\right)^I \tag{68}$$

$$\Im\left(FRF_{jk}\right)^I = \sum_{i=1}^{n} \Im\left(FRF_{jk}^i\right)^I \tag{69}$$

The result of the summation is an interval range for the real and imaginary part of the complex response for every frequency. This means that it defines a rectangle in the complex space in which the response vector is contained. Based on this rectangle, an approximation of the amplitude range of the complex response is easily obtained by taking the points on the rectangle which are respectively the nearest and most distant from the origin.

4 Numerical example

The presented methodology is now illustrated on a realistic case study. The model under investigation represents a car windshield in free-free conditions. The windshield is composed of five layers: two outer glass layers, and three inner layers of various polymers. During manufacturing, the thicknesses of these layers are subject to tolerances. The tolerances are defined as a range of thickness for the total of the five layers, and a range of total thickness for the inner polymer layers. Furthermore, damping variation has been detected from experiments. The aim of this case study is to analyze the effect of the manufacturing design tolerances in combination with the damping uncertainty on the dynamical behavior of the windshield.

Figure 20 shows the nominal finite element model of the windshield (courtesy of Renault, France). The model contains a total of 798 elements. In the dynamic response analysis, a direct drive point FRF along the Z-direction is considered, with the input and response location as indicated in figure 20. At this location, the components of the force and displacement normal to the surface are considered. The response is analyzed up to a frequency of 180 Hz, which corresponds to the range covered by the 15 first modes.

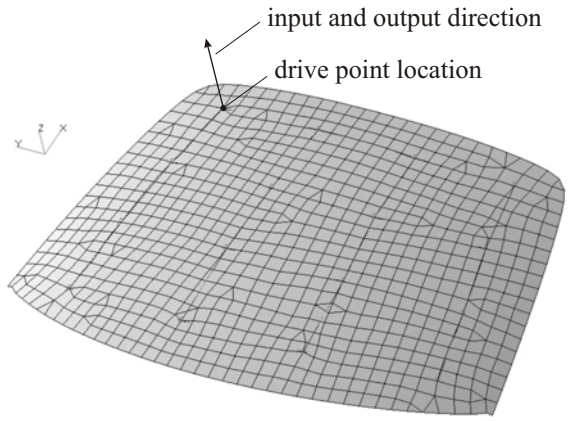

Figure 20: Nominal finite element model of the windshield, with indication of the response location of the direct FRF

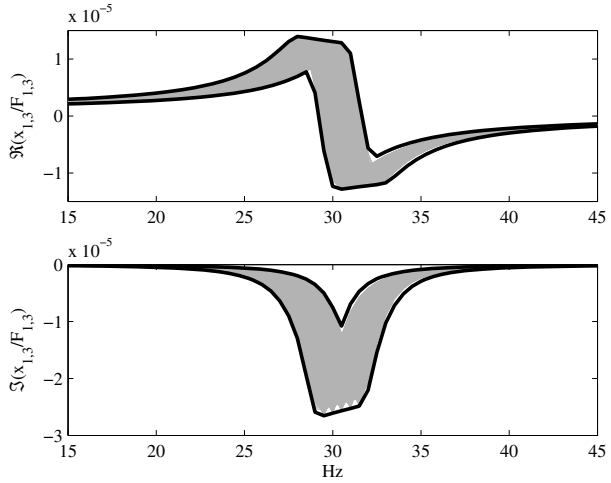

Figure 21: Predicted modal real and imaginary envelope FRF of the third mode (black), compared to 1000 samples randomly generated over the interval uncertainty space (grey)

The windshield is modeled using layered composite elements, the individual layer thicknesses of which are parametrized in order to perform the global optimization on the modal parameters, necessary for the MRE $\langle \hat{k}_i, \hat{m}_i \rangle$-domain approximation. The damping uncertainty is added to the analysis as an individual uncertain modal damping parameter for each mode under consideration in the modal superposition. The modal damping factors are derived from a total of three experiments performed on three different realizations of the windshield. In the interval analysis, the modal damping uncertainty is quantified as the interval enveloping these experimental modal damping factors. This brings the total of independent uncertain parameters to 17 (2 layer thicknesses, 15 modal damping factors).

Figure 21 illustrates the modal real and imaginary envelope FRF for the third mode resulting from the procedure as described in section 3 of this paper. As a verification, a total of 1000 samples has been generated, resulting in the cloud of response curves (grey lines in the figure). The samples result from a Monte Carlo-simulation using a uniform distribution over the tolerance and modal damping intervals. This figure clearly indicates that for this mode, the procedure introduced above finds conservative but very tight bounds on the dynamic response range under the given interval uncertainty.

Figure 22 finally shows the total amplitude envelope response function obtained with the presented methodology. Again, the total envelopes are compared to the samples generated with the Monte Carlo-procedure. Also here, the predicted bounds are conservative, but give a good indication of the upper bound on the feasible response range. Especially in the critical area where the response of the structure is high, the envelope describes very tight bounds around the sampled response functions. From these results, conclusions can be drawn regarding the possible dynamic behavior of the structure, given the uncertain interval bounds on specific model properties. This can be very valuable information for a designer who is interested in the combined effect of defined tolerances and damping variability on the dynamic behavior of his design.

5 Conclusions

This paper explains how the hybrid optimization – interval arithmetic procedure developed for dynamic response analysis of undamped structures can be extended to the analysis of structures with uncertain modal damping factors. The developed procedure adopts the hybrid interval translation of the modal superposition principle, including

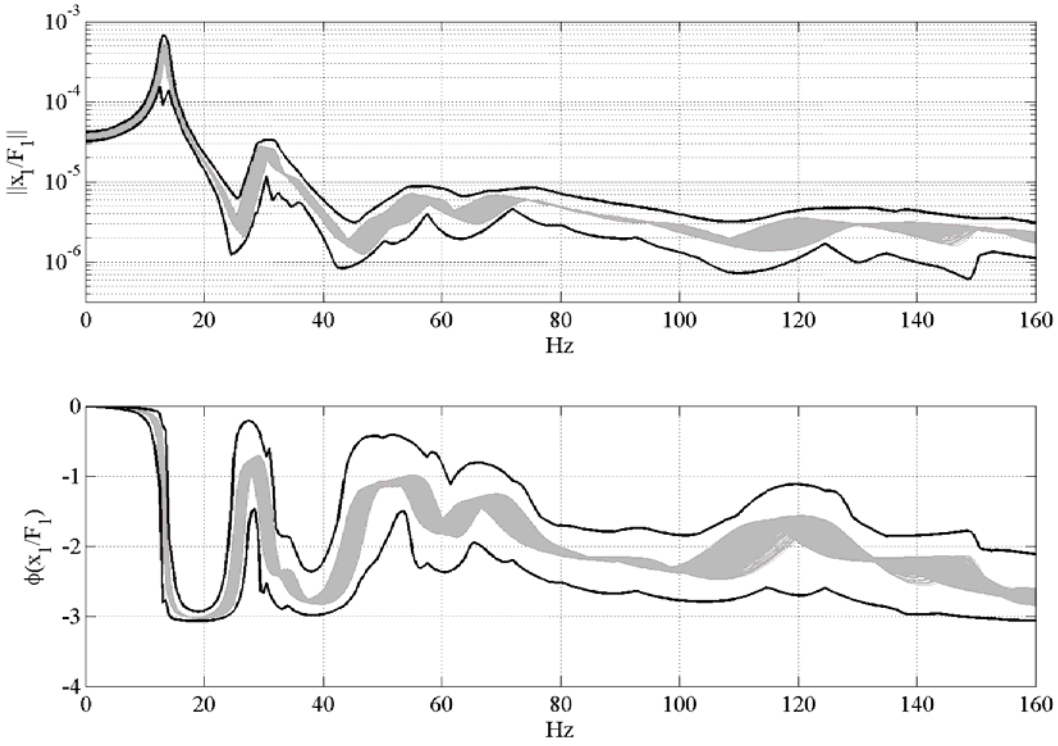

Figure 22: Predicted amplitude and phase envelope FRF (black), compared to 1000 samples randomly generated over the interval uncertainty space (grey)

the modal rectangle method with eigenvalue interval correction. Addition of an independent modal damping interval to the analysis results in a three-dimensional modal domain. The modal parameter range of each mode is extended in the modal damping direction. The range of the real and imaginary parts of the modal contributions to the total frequency response function are calculated, by taking into account that the modal parameter triplets can be anywhere within this extended modal parameter range. This results in an analytical procedure, which proves to be highly efficient. The main advantage of the developed procedure is that the modal damping intervals are introduced directly into the interval arithmetic part of the procedure. This means that there is no extra preliminary optimization necessary. Consequently, the computational efficiency of the procedure is hardly affected with respect to the undamped case.

The effect of uncertain geometric parameters in combination with experimentally identified modal damping uncertainty on the dynamic behavior of a car windshield is analyzed. This analysis shows the efficiency and correctness of the procedure. Thanks to the efficient analytical treatment of modal damping intervals, a relatively high amount of independent interval uncertainties can be analyzed. In the treated example, 17 independent interval parameters are present, 15 of which are modal damping parameter uncertainties. The resulting envelopes on the response function of the windshield prove to be very useful for dynamic assessment of the structure under uncertain conditions.

Acknowledgement: The author is supported by the Research Foundation - Flanders as a post-doctoral research fellow. Part of this research was conducted with financial support of the European Commission through the Marie Curie Research & Training Network MRTN-CT-2003-505164, MADUSE: Modelling Product Variability and Data Uncertainty in Structural Dynamics Engineering.

References

Chen, L.; Rao, S. (1997): Fuzzy finite-element approach for the vibration analysis of imprecisely-defined systems. *Finite Elements in Analysis and Design*, vol. 27, pp. 69–83.

Dessombz, O.; Thouverez, F.; Laîné, J.; Jézéquel, L. (2001): Analysis of mechanical systems using interval computations applied to finite element methods. *Journal of Sound and Vibration*, vol. 239, no. 5, pp. 949–968.

Donders, S.; Vandepitte, D.; Van de Peer, J.; Desmet, W. (2005): Assessment of uncertainty on structural dynamic responses with the short transformation method. *Journal of Sound and Vibration*, vol. 288, no. 3, pp. 523–549.

Elishakoff, I. (2000): Possible limitations of probabilistic methods in engineering. *ASME Applied Mechanics Reviews*, vol. 53, no. 2, pp. 19–36.

Hanss, M. (2003): The extended transformation method for the simulation and analysis of fuzzy-parameterized models. *International Journal of Uncertainty Fuzziness and Knowledge-Based Systems*, vol. 11, no. 6, pp. 711–727.

Köylüoğlu, U.; Çakmak, A.; Nielsen, S. (1995): Interval algebra to deal with pattern loading and structural uncertainties. *Journal of Engineering Mehanics*, vol. 121, no. 11, pp. 1149–1157.

Massa, F.; Tison, T.; Lallemand, B. (2006): A fuzzy procedure for the static design of imprecise structures. *Computer Methods in Applied Mechanics and Engineering*, vol. 195, no. 9-12, pp. 925–941.

Moens, D.; Vandepitte, D. (2004): An interval finite element approach for the calculation of envelope frequency response functions. *International Journal for Numerical Methods in Engineering*, vol. 61, no. 14, pp. 2480–2507.

Moens, D.; Vandepitte, D. (2005): A survey of non-probabilistic uncertainty treatment in finite element analysis. *Computer Methods in Applied Mechanics and Engineering*, vol. 194, no. 14-16, pp. 1527–1555.

Muhanna, R.; Mullen, R.; Zhang, H. (2005): Penalty-based solution for the interval finite-element methods. *Journal of Engineering Mechanics-Asce*, vol. 131, no. 10, pp. 1102–1111.

Mullen, R.; Muhanna, R. (1999): Bounds of structural response for all possible loading combinations. *Journal of Structural Engineering*, vol. 125, no. 1, pp. 98–106.

Neumaier, A. (2006): Linear systems with large uncertainties, with applications to truss structures. *Reliable Computing*. to appear.

Qiu, Z.; Wang, X.; Chen, J. (2006): Exact bounds for the static response set of structures with uncertain-but-bounded parameters. *International Journal of Solids and Structures*, vol. 43, pp. 6574–6593.

Rao, S.; Sawyer, J. (1995): Fuzzy finite element approach for the analysis of imprecisely defined systems. *AIAA Journal*, vol. 33, no. 12, pp. 2364–2370.

Stroud, W.; Krishnamurthy, T.; Smith, S. (2002): Probabilistic and possibilistic analyses of the strength of a bonded joint. *CMES: Computer Modelling in Engineering & Sciences*, vol. 3, no. 6, pp. 755–772.

Wasfy, T.; Noor, A. (1998): Application of fuzzy sets to transient analysis of space structures. *Finite Elements in Analysis and Design*, vol. 29, pp. 153–171.